Lateral Diffusion and Signaling of Receptor for Advanced Glycation End-products (RAGE): A Receptor Involved in Chronic Inflammation

Aleem Syed[1], Qiaochu Zhu[1] and Emily A. Smith

Department of Chemistry, Iowa State University, 1605 Gilman Hall, Ames, IA 50011

1 Both authors contributed equally

*esmith1@iastate.edu, (+1) 515-294-1424 (P), (+1) 515-294-0105 (F)

Abstract

Membrane diffusion is one of the key mechanisms in the cellular function of receptors. The signaling of receptor for advanced glycation end-products (RAGE) has been extensively studied in the context of several pathological conditions, however, very little is known about RAGE diffusion. To fill this gap, RAGE lateral diffusion is probed in native, cholesterol depleted and cytoskeleton altered cellular conditions. In native GM07373 cellular conditions, RAGE has a 90% mobile fraction and an average diffusion coefficient of 0.3 $\mu m^2/s$. When depolymerization of the actin cytoskeleton is inhibited with the small molecule Jasplakinolide (Jsp), the RAGE mobile fraction and diffusion coefficient decrease by 22% and 37%, respectively. In contrast, depolymerizing the filamentous actin cytoskeleton using the small molecule cytochalasin D (CD) does not alter the RAGE diffusion properties. There is a 70% and 50% decrease in phosphorylation of extracellular signal-regulated kinase (p-ERK) when the actin cytoskeleton is disrupted by CD or Jsp in RAGE expressing GM07373 cells. Disrupting the actin cytoskeleton in GM07373 cells that do not express detectable amounts of RAGE results in no change in p-ERK. Cholesterol depletion results in no statistically significant change in the diffusion properties of RAGE or p-ERK. This work presents a strong link between the actin cytoskeleton and RAGE diffusion and downstream signaling, and serves to further our understanding of the factors influencing RAGE lateral diffusion.

Keywords Fluorescence recovery after photobleaching, phosphorylation of ERK, cell membrane biophysics, actin cytoskeleton, cholesterol depletion

Introduction

Lateral diffusion of membrane proteins is often interrelated with their cellular signaling and functions in the cell membrane (Axelrod 1983; Ganguly *et al.* 2008; Ronchi *et al.* 2008). The receptor for advanced glycation endproducts (RAGE) is a transmembrane protein that belongs to the immunoglobulin (Ig) superfamily. Many RAGE ligands have been identified, including advanced glycation endproducts (AGEs), S100 proteins, high mobility group box 1 (HMGB1), and amyloid-β fibrils (Koch *et al.* 2010; Leclerc *et al.* 2009; Schmidt *et al.* 1992; Taguchi *et al.* 2000; Yan *et al.* 1996). RAGE and its signaling are associated with many disease states, including some types of cancer, retinal disease, cardiovascular disease, Alzheimer's disease, respiratory disorders, chronic inflammation and diabetic complications (Barile and Schmidt 2007; Basta 2008; Bierhaus and Nawroth 2009; Briot *et al.* 2009; Hofmann *et al.* 1999; Logsdon *et al.* 2007; Yan *et al.* 2009). RAGE is reported to activate various signaling cascades, including mitogen-activated protein kinases (MAPKs), Rac/Cdc42 and Janus kinases (JAK)/signal transducers and activators of transcription (STATs) and NF-κB (Ghavami *et al.* 2008; Hermani *et al.* 2006; Huttunen *et al.* 1999; Lander *et al.* 1997; Wang *et al.* 2008; Yeh *et al.* 2001). Through these signaling pathways, RAGE influences cell survival, motility and the inflammatory response. Even though RAGE signaling has been studied extensively in different disease states, very little is reported regarding RAGE diffusion in the cell membrane. The goal of the current study is to investigate the lateral diffusion and cellular signaling of RAGE in the endothelial cell membrane and to study the effects of cholesterol depletion and alterations to the actin cytoskeleton on these properties.

Cholesterol and the actin cytoskeleton play an important role in the organization of the cell membrane. Functional domains in the cell membrane, known as lipid rafts or lipid

53 nanodomains, contain about 3 to 5-fold excess cholesterol compared to neighboring regions of
54 bilayer (Ando *et al.* 2015; Lingwood and Simons 2010; Pike 2003; Simons and Gerl 2010).
55 These functional domains act as platforms for localizing and signaling of many membrane
56 proteins. Altering membrane cholesterol levels has been reported to affect the organization and
57 signaling of a number of receptors (Adkins *et al.* 2007; Arora *et al.* 2014; Bag *et al.* 2015; Brown
58 and London 1998; Pike 2003; Pucadyil and Chattopadhyay 2006). The actin cytoskeleton serves
59 as a structural element that can affect the functionality of membrane proteins, including their
60 oligomerization and transmembrane signaling (Kusumi *et al.* 2011).

61 Both cholesterol and the actin cytoskeleton have been reported to play a key role in
62 RAGE functions. For example Reddy *et al.* showed cholesterol depletion inhibited the S100-
63 induced effects involving RAGE in vascular smooth muscle cells and that intact caveolae are
64 necessary for RAGE signaling (Reddy *et al.* 2006). RAGE has also been reported to be part of
65 functional cholesterol-enriched domains in neural endothelial cells (Lisanti *et al.* 1994; Sbai *et*
66 *al.* 2010). Xiong *et al.* showed that the actin cytoskeleton played a pivotal role in RAGE-
67 mediated plasma membrane plasticity in a human umbilical vein endothelial cell line (Xiong *et*
68 *al.* 2011). They found that RAGE over expression reorganizes filamentous actin (F-actin) by
69 increasing β-catenin levels, resulting in inhibition of membrane sealing. Although it is evident
70 that cholesterol and the actin cytoskeleton affect some RAGE functions, possible roles in
71 affecting RAGE lateral diffusion remain unknown.

72 In this study, we have genetically fused monomeric red fluorescent protein (mRFP) to the
73 C-terminus of RAGE and measured its lateral diffusion using fluorescence recovery after
74 photobleaching (FRAP) in GM07373 endothelial cells. In FRAP, a small area on the cell
75 membrane is photobleached with a focused laser beam and the fluorescence recovery from the

diffusion of neighboring fluorescent molecules into the photobleached spot is recorded over time. Several models have been constructed to extract diffusion parameters such as the immobile population, diffusion coefficient and time-dependency of the diffusion (Feder *et al.* 1996; van Zoelen *et al.* 1983). RAGE diffusion at native, cholesterol depleted and altered actin cytoskeleton conditions have been studied. Methyl-β-cyclodextrin (MβCD) was used to deplete cellular cholesterol. The actin cytoskeleton was altered using cytoskeletal drugs cytochalasin D (CD) and Jasplakinolide (Jsp). Finally, signaling was measured by quantifying the phosphorylation of extracellular-signal-regulated kinase (p-ERK) at native and altered cellular conditions.

MATERIALS & METHODS

Cell culture

All experiments were performed using bovine artery GM07373 endothelial cells (Coriell Institute Biorepositories, Camden, NJ). GM07373 cells were grown in complete growth medium consisting of Dulbecco's modified Eagle's medium (DMEM) (Sigma-Aldrich, St. Louis, MO), 10% fetal bovine serum (FBS) (Irvine Scientific, Santa Ana, CA) and 12.5 mM Streptomycin and 36.5 mM Penicillin (Fisher Scientific, Pittsburgh, PA) in a water-jacketed CO_2 incubator (Thermo Scientific, Waltham, MA). Cells were sub-cultured using 0.25% (w/v) trypsin-EDTA (Life Technology, Carlsbad, CA) solution every two days. All transfected GM07373 cells were established to express respective recombinant proteins stably before any microscopy or molecular biology experiments were performed. Plasmid and transfection details are in the supplementary information.

98

99 Western blotting

100 GM07373 cells expressing RAGE (GM07373-RAGE) or RAGE-mRFP (GM07373-RAGE-
101 mRFP) were cultured to 100% confluence and rinsed with ice cold phosphate buffered saline
102 (PBS). Cells were lysed with RIPA buffer (150 mM sodium chloride, 1.0% NP-40 detergent,
103 0.5% sodium deoxycholate, 0.1% SDS, 50 mM Tris, pH 8.0) with Halt™ protease inhibitor
104 cocktail (1×, Thermo Scientific, Rockford, IL). After the initial lysis treatment, cells were passed
105 through a 21 gauge needle to ensure complete cell lysis. The protein mixture was first separated
106 on the NuPAGE® Novex® 4-12% Bis-Tris protein gel (Life Technology, Eugene, OR) and then
107 electro blotted onto Immun-Blot® LF PVDF membrane (Bio-Rad, Hercules, CA) as described
108 previously (Matsudaira 1989; Towbin *et al.* 1979). The PVDF membrane was probed following
109 the manufacturer's protocol (Bio-Rad). Antibodies used for probing were: anti-RAGE rabbit (H-
110 300, Santa Cruz Biotechnology), anti-RFP rabbit (Life Technology), anti-Vinculin goat (sc-7649,
111 Santa Cruz Biotechnology), anti-Actin rabbit (sc-1616-R, Santa Cruz Biotechnology), anti-p-
112 ERK rabbit (Tyr 204, sc-101761, Santa Cruz Biotechnology), anti-total-ERK 1/2 mouse (sc-
113 514302, Santa Cruz Biotechnology). The labeled secondary antibodies were Alexa Fluor 647
114 goat anti-rabbit (Life technologies), Alexa Fluor 488 donkey anti-goat (Life technologies), Alexa
115 Fluor 488 goat anti-mouse (Life technologies). Fluorescence was measured on a Typhoon FLA
116 9500 variable mode laser scanner (GE Healthcare, Waukesha, WI). The total-ERK and vinculin
117 protein bands were used as a loading control in Western blot experiments. The fluorescence
118 intensities were calculated from the 42 kDa band of p-ERK divided by the 42 kDa band of total-
119 ERK or the 42 kDa band of actin divided by the 130 kDa band of vinculin. The 42 kDa band of
120 ERK was used since it has a stronger intensity than the 44 kDa ERK band. All experiments were

performed in triplicate unless otherwise noted in figure legends. Reported p values were calculated using the Student's t-test with a two-tailed homoscedastic distribution. Protein sequences were analyzed by mass spectrometry as reported in the supplemental information.

FRAP sample preparation

Sterile glass bottom culture dishes were made by attaching a cover glass (22mm × 22mm, No. 1.5, Corning Inc., Corning, NY) to the bottom of a polystyrene petri dish (35mm × 10mm, Fisher Scinetific) containing a pre-drilled 3/4 inch diameter hole as described previously (Buster *et al.* 2010). GM07373-RAGE or GM07373-RAGE-mRFP cells were sub-cultured onto the culture dishes two days before the experiment. Cells were either used without further treatment or treated at 37 ºC with MβCD (Sigma-Aldrich, 5mM, in serum free DMEM for 30 minutes) to deplete the cholesterol or with CD (Sigma-Aldrich, 10 μM, in serum free DMEM for 60 minutes) or with Jsp (Santa Cruz Biotechnology, 3μM, in serum free DMEM for 30 minutes) to alter the actin cytoskeleton as previously reported (Arora *et al.* 2014; Schwab *et al.* 2003; Shaw and Tilney 1999) before the FRAP experiments.

FRAP Microscopy

All FRAP experiments were performed on a Nikon Eclipse TE2000U inverted microscope (Nikon, Melville, NY) which was equipped with an oil-immersion objective (100×, Apo TIRF, 1.49 numerical aperture). The microscope was housed in a home built 0.9×0.6×0.5 m^3 Plexiglas box containing a heat source to maintain a 36 ± 2 ºC at the sample throughout the experiment. Fluorescence was excited with a mercury lamp (X-cite 120 PC, EXFO Photonic Solutions Inc., Mississauga, Ontario, Canada) operating at 25% of the power and an excitation filter

144 (HQ545/30x, Chroma Technology Corp., Bellows Falls, VT). The resulting fluorescence
145 emission was collected through an emission filter (HQ620/60x, Chroma Technology Corp.). For
146 photobleaching a region of the cell membrane, a 488-nm laser was directed to the sample with a
147 dichroic mirror (Q495lp, Chroma Technology Corp.). The laser power and photobleaching spot
148 diameter at the sample were 10 mW and 4.0 μm, respectively. A LabView program (National
149 Instruments, Austin, TX) was developed to control a shutter (Thorlabs, Jessup, MD) in the laser
150 path. The photobleaching time was 2 msec. Fluorescence images were recorded using a
151 PhotonMAX 512B EMCCD camera (Princeton Instruments, Trenton, NJ) and Winview
152 (Photometric, Tucson, AZ) image acquisition software. Ten pre-photobleach and 100 post-
153 photobleach images were collected with a time resolution of 410 ms per image. Dark-state
154 formation in mRFP is expected to have a negligible impact on the FRAP data collected on this
155 timescale. Data collection was completed within 1 h after adding imaging medium (pH=7.2, 155
156 mM NaCl, 5 mM KCl, 2 mM $CaCl_2$, 1 mM $MgCl_2$, 2 mM NaH_2PO_4, 10 mM HEPES and 10 mM
157 Glucose) to the cells.
158
159 FRAP data analysis
160 The fluorescence images collected pre-photobleach and post-photobleach were analyzed with
161 ImageJ (version 1.48, National Institute of Health) software. The fluorescence intensity from
162 three regions of interest (ROIs) was extracted for each image in the series of 110 images. The
163 ROIs were classified as the photobleached region (an area on the plasma membrane illuminated
164 by the laser spot), the non-photobleached region (an area on the plasma membrane away from
165 the photobleached region), and the background (an area where there was no cell present in the
166 field of view). Fluorescence recovery curves were constructed with a three-step process: (i) the

background intensity was subtracted from fluorescence intensities in the photobleached ROI, the resulting curves were normalized with the fluorescence intensities from (ii) the non-photobleached ROI and (iii) the average pre-photobleached intensity from the subsequently photobleached region to account for the lamp intensity fluctuations as well as photobleaching during the image acquisition period as described by Phair *et al.* (Phair *et al.* 2004). Fluorescence recovery curves were analyzed and the results were averaged over 24 to 53 cells for each data set. The number of cells measured was lower for Jsp, CD and MβCD data sets. These treatments result in a smaller average spread cell diameter, which reduces the number of cells that can be analyzed by FRAP compared to the untreated cells. Mobile fractions (*MF*) were calculated using equation 1.

$$MF = \frac{F_\infty - F_0}{F^0 - F_0} \times 100 \qquad (1)$$

Where F_0 is the intensity immediately after photobleaching, F^0 is the pre-photobleaching intensity and F_∞ is the final intensity (i.e., in image 110), where all fluorescence intensities refer to the values from the fluorescence recovery curves. Each fluorescence recovery curve was further fit to equation 2 using IGOR Pro V 6.32A (WaveMetrics Inc., Lake Oswego, OR) to measure the time dependency of the fluorescence recovery as well as diffusion coefficients (Feder *et al.* 1996).

$$F(t) = \frac{F_o + F_\infty \left(\frac{t}{\tau}\right)^\alpha}{1 + \left(\frac{t}{\tau}\right)^\alpha} \qquad (2)$$

Where $F(t)$ is the fluorescence intensity at time t, α is the time exponent and τ is time for 50% fluorescence recovery. Diffusion coefficients were calculated using equation 3.

$$D(t) = \frac{\omega^2}{4\tau^\alpha t^{(\alpha-1)}} \qquad (3)$$

Where $D(t)$ is the diffusion coefficient at time t and ω is the radius of the photobleached spot. The statistical significance of all reported data sets was calculated using first the F-test at the 95% confidence level and then the homoscedastic/heteroscedastic (as determined from the F-test) Student's t-test with a two-tailed distribution. The resulting p values that indicate statistical differences are reported in Figure 7; statistical differences at the 95% confidence level (i.e., p values below 0.05) are considered significant. Diffusion parameters are presented as box-and-whisker plots. For box-and-whisker plots, the boundary of the box shows the twenty-fifth and seventy-fifth quartiles. A line and a triangle within the box indicate the median and the mean, respectively. Whiskers above and below the boxes are 1.5 times the interquartile range.

Actin cytoskeleton staining

Cells were sub-cultured onto glass-bottom petri dishes and allowed to spread in the incubator for two days before the experiment. Cells were treated as described above with 5 mM MβCD, 10 μM CD, or 3 μM Jsp before the actin cytoskeleton was stained for fluorescence imaging. The staining protocol was described previously (Syed *et al.* 2014). Briefly, cells were fixed with 4% (w/v) paraformaldehyde in PBS for 10 minutes. Triton X-100 (0.1% (v/v) in PBS) was used for cell membrane permeabiliztion. Blocking was performed using bovine serum albumin (1% (w/v) in PBS) for 5 minutes. Cells were further incubated with Atto 647N conjugated phalloidin (Sigma-Aldrich) to stain the F-actin overnight at 4 °C. Stained cells were rinsed with imaging medium before imaging using the Nikon Eclipse TE2000U inverted microscope described above. The actin cytoskeleton was further quantified to measure the alignment in the actin fibers in 21 to 41 cells. Alignment was calculated using an ImageJ plugin, FibrilTool, as described previously (Boudaoud *et al.* 2014).

Results and Discussion

Characterization of RAGE and RAGE-mRFP Expression

The primary goal of this study is to probe the lateral diffusion of RAGE in the GM07373 cell membrane in order to characterize the role of the actin cytoskeletal and cholesterol in altering RAGE diffusion. To achieve this goal, plasmids were transfected into GM07373 cells to stably express full-length RAGE or RAGE-mRFP. RAGE or RAGE-mRFP expression was confirmed by Western blot analysis of cell lysates as shown in Fig. 1. A protein band corresponding to RAGE at ~55 kDa (band 1, Fig. 1) was observed in the GM07373-RAGE cell lysate (lane b, Fig. 1) but not in the GM07373 cell lysate (lane a, Fig. 1). Surprisingly, the GM07373-RAGE-mRFP cell lysate (lane c, Fig. 1) showed three bands in the 60 to 80 kDa molecular weight range after probing the membrane with the RAGE primary antibody. Bands 1 to 4 were positive for RAGE peptides as measured by mass spectrometry. After the PVDF membrane was probed with a polyclonal mRFP antibody, only a single band was observed from the GM07373-RAGE-mRFP cell lysate (band 5, Fig. 1) near the molecular weight of band 3. It was confirmed by fluorescence imaging of the PVDF membrane that fluorescence was measured only at the location of band 5, thus RAGE-containing bands 2 and 4 do not contribute to the fluorescence microscopy results reported below.

Phosphorylation of extracellular-signal-regulated kinase (p-ERK) was used as a marker for downstream RAGE signaling (Huttunen *et al.* 2002; Zong *et al.* 2010). There was no statistically significant difference in p-ERK levels in cells expressing RAGE or RAGE-mRFP

(Fig. 2), indicating that the mRFP tag on RAGE did not alter p-ERK signaling in GM07373 cells.

RAGE-mRFP diffusion in the native GM07373 cell membrane

FRAP experiments on GM07373 cells expressing RAGE-mRFP were performed and the average recovery curve from 24-53 cells is shown in Online Resource 1 (Fig. S1). Each replicate curve was individually fit to the time-dependent diffusion model with an immobile fraction (i.e., all parameters α, F_0, F_∞ and τ in equation 2 were allowed to vary) as described by Federer *et al.* (Feder *et al.* 1996). The time exponent (α) from the fit parameters provides information on the nature of the mode of diffusion. An α value of 1 indicates time-independent Brownian diffusion, whereas a value less than 1 indicates time-dependent diffusion. The average α value measured for RAGE-mRFP was 0.9 (Fig. 7). The average mobile fraction was 90% and the average diffusion coefficient was 0.3 $\mu m^2/s$ for RAGE-mRFP at native cellular conditions. While FRAP provides a measure of the average diffusion properties of RAGE-mRFP, it is known that RAGE diffusion is heterogeneous (Syed *et al.* 2016). For example, when the diffusion coefficient is measured one receptor at a time across 100 receptors, the diffusion coefficient varies by over 4 orders of magnitude. The heterogeneity in RAGE diffusion is not detectable with the ensemble FRAP method. On the other hand, FRAP measurements yield the fraction of mobile RAGE, which has not been possible to measure with other analysis techniques (Syed *et al.* 2016).

Alterations to the F-actin cytoskeleton alter RAGE-mRFP diffusion properties measured by FRAP

To study the possible effect of the actin cytoskeleton on RAGE lateral diffusion, the actin cytoskeleton was altered with two drugs, CD and Jsp. CD depolymerizes the filamentous actin cytoskeleton and prevents repolymerization by binding to actin monomers (Casella *et al.* 1981). Jsp binds with filamentous actin and inhibits depolymerization (Spector *et al.* 1999). Atto 647N conjugated phalloidin was used to measure the effect of CD and Jsp on the actin cytoskeleton in GM07373-RAGE cells as shown in Fig. 3. In the native GM07373 cells, the actin cytoskeleton staining generated partially aligned fibers with a well-defined cell boundary as shown in Fig. 3a. After the CD treatment, the actin structure was significantly altered and no clear cell boundary was observed (Fig. 3c). Jsp binds to the actin cytoskeleton in competition with the Atto 647N conjugated phalloidin (Bubb *et al.* 2000). Hence, Atto 647N phalloidin actin cytoskeleton staining was diminished for Jsp treated cells (Fig. 3d). There was no change in the actin expression as measured from Western blot analysis of the cell lysate treated with CD or Jsp (Fig. 4).

RAGE-mRFP diffusion parameters were measured for CD or Jsp treated cells. The RAGE-mRFP mobile fraction and diffusion coefficient were decreased by 22% and 37%, respectively, when the actin cytoskeleton was altered with Jsp (Fig. 7). In contrast, CD treatment does not alter the RAGE diffusion properties. Jsp and CD have opposite effects on the polymerization of the actin cytoskeleton. Jsp hinders depolymerization, whereas CD depolymerizes the actin filaments. Jsp results in less mobile and slower RAGE, suggesting an actin cytoskeleton fixed in a polymerized state slows RAGE diffusion and reduces the mobile fraction. Surprisingly, CD treatment to depolymerize the actin cytoskeleton does not statistically increase RAGE mobility as measured by FRAP; although it is noteworthy that prior to altering

279 the actin cytoskeleton RAGE diffusion is already relatively unhindered with a large mobile
280 fraction and nearly Brownian behavior as indicated by the α value.

281 To understand if RAGE diffusion properties are linked to downstream signaling,
282 phosphorylation of ERK (p-ERK) was measured in both GM07373 and GM07373-RAGE cells
283 after CD and Jsp treatment. p-ERK was decreased by 70% and 50% in GM07373-RAGE cells
284 when the actin cytoskeleton was disrupted with CD and JSP, respectively (Fig. 5a and b). There
285 was no statistically significant change in p-ERK observed in GM07373 cells lacking detectable
286 RAGE expression after CD or Jsp treatment (Fig. 5c and d). This indicates that the downstream
287 signaling of RAGE is altered when the actin cytoskeleton is disrupted, regardless of the effects
288 disrupting the actin cytoskeleton has on RAGE diffusion.

289 To investigate the effect of cholesterol on the lateral diffusion of RAGE-mRFP,
290 cholesterol was depleted using MβCD. The total free cholesterol was depleted by 45% and no
291 statistically significant change in the endogenous cholesterol ester was observed when cells were
292 incubated with 5 mM MβCD as measured by Amplex® Red cholesterol quantification assay
293 (Fig. 6a). The diffusion parameters statistically unchanged for RAGE-mRFP (Fig. 7). There was
294 also no change in p-ERK measured after cholesterol depletion from both GM07373-RAGE cells
295 and GM07373 (Fig. 6b-d). These conclusions are valid in the absence of RAGE ligand. In the
296 presence of ligand, RAGE signaling may be dependent on cholesterol as previously reported
297 (Reddy *et al.* 2006).

298 It has been previously reported that a change in membrane cholesterol not only affects the
299 cell membrane structure but also has a global effect, including reorganization of the actin
300 structure (Kwik *et al.* 2003). This appears to be valid in GM07373-RAGE cells (Fig. 3 a and b).

A significant 40% decrease in the actin fiber alignment was measured after cholesterol depletion in both the GM07373-RAGE and GM07373 cell lines. No change in the actin expression was observed with cholesterol depletion (Fig. 6). These observations indicate that cholesterol depletion affects the actin cytoskeleton organization, but the cholesterol-depletion-induced changes to the actin cytoskeleton alignment are not associated with changes in RAGE diffusion properties.

In summary, RAGE-mRFP diffuses in the cell membrane with a large mobile fraction at native GM07373 cellular conditions. The depolymerization of the actin cytoskeleton plays a role in how RAGE diffuses in the membrane, and more generally, the actin cytoskeleton polymerization dynamics alter the downstream signaling of RAGE. Even though there is a significant change in the actin cytoskeleton alignment as revealed by phalloidin staining, cholesterol depletion has no effect on RAGE lateral diffusion as measured by FRAP or signaling as measured by p-ERK. The combined data point to an important role for actin depolymerization in the diffusion properties of RAGE and a link between the actin cytoskeleton and RAGE-mediated p-ERK signaling.

Acknowledgements

This work was supported by the National Science Foundation (CHE- 1412084). The authors thank Joel Nott of the protein facility at Iowa State University for help with mass spectrometry, and Dipak Mainali and Chamari Wijesoorya for their assistance with cell culture.

References

Adkins EM, Samuvel DJ, Fog JU, Eriksen J, Jayanthi LD, Vaegter CB, Ramamoorthy S, Gether U (2007) Membrane mobility and microdomain association of the dopamine transporter studied with fluorescence correlation spectroscopy and fluorescence recovery after photobleaching. Biochemistry 46:10484-10497

Ando J, Kinoshita M, Cui J, Yamakoshi H, Dodo K, Fujita K, Murata M, Sodeoka M (2015) Sphingomyelin distribution in lipid rafts of artificial monolayer membranes visualized by Raman microscopy. Proc Natl Acad Sci U S A 112:4558-4563

Arora N, Syed A, Sander S, Smith EA (2014) Single particle tracking with sterol modulation reveals the cholesterol-mediated diffusion properties of integrin receptors. Phys Biol 11:066001

Axelrod D (1983) Lateral motion of membrane proteins and biological function. Journal of Membrane Biology 75:10

Bag N, Huang S, Wohland T (2015) Plasma Membrane Organization of Epidermal Growth Factor Receptor in Resting and Ligand-Bound States. Biophys J 109:1925-1936

Barile GR, Schmidt AM (2007) RAGE and its ligands in retinal disease. Curr Mol Med 7:758-765

Basta G (2008) Receptor for advanced glycation endproducts and atherosclerosis: From basic mechanisms to clinical implications. Atherosclerosis 196:9-21

Bierhaus A, Nawroth PP (2009) Multiple levels of regulation determine the role of the receptor for AGE (RAGE) as common soil in inflammation, immune responses and diabetes mellitus and its complications. Diabetologia 52:2251-2263

Boudaoud A, Burian A, Borowska-Wykret D, Uyttewaal M, Wrzalik R, Kwiatkowska D, Hamant O (2014) FibrilTool, an ImageJ plug-in to quantify fibrillar structures in raw microscopy images. Nat Protoc 9:457-463

Briot R, Frank JA, Uchida T, Lee JW, Calfee CS, Matthay MA (2009) Elevated levels of the receptor for advanced glycation end products, a marker of alveolar epithelial type I cell injury, predict impaired alveolar fluid clearance in isolated perfused human lungs. Chest 135:269-275

Brown DA, London E (1998) Functions of lipid rafts in biological membranes. Annu Rev Cell Dev Biol 14:111-136

Bubb MR, Spector I, Beyer BB, Fosen KM (2000) Effects of jasplakinolide on the kinetics of actin polymerization. An explanation for certain in vivo observations. J Biol Chem 275:5163-5170

Buster DW, Nye J, Klebba JE, Rogers GC (2010) Preparation of Drosophila S2 cells for light microscopy. J Vis Exp

Casella JF, Flanagan MD, Lin S (1981) Cytochalasin D inhibits actin polymerization and induces depolymerization of actin filaments formed during platelet shape change. Nature 293:302-305

Feder TJ, Brust-Mascher I, Slattery JP, Baird B, Webb WW (1996) Constrained diffusion or immobile fraction on cell surfaces: a new interpretation. Biophys J 70:2767-2773

Ganguly S, Pucadyil TJ, Chattopadhyay A (2008) Actin cytoskeleton-dependent dynamics of the human serotonin1A receptor correlates with receptor signaling. Biophys J 95:451-463

Ghavami S, Rashedi I, Dattilo BM, Eshraghi M, Chazin WJ, Hashemi M, Wesselborg S, Kerkhoff C, Los M (2008) S100A8/A9 at low concentration promotes tumor cell growth via RAGE ligation and MAP kinase-dependent pathway. J Leukoc Biol 83:1484-1492

Hermani A, De Servi B, Medunjanin S, Tessier PA, Mayer D (2006) S100A8 and S100A9 activate MAP kinase and NF-kappaB signaling pathways and trigger translocation of RAGE in human prostate cancer cells. Exp Cell Res 312:184-197

Hofmann MA, Drury S, Fu C, Qu W, Taguchi A, Lu Y, Avila C, Kambham N, Bierhaus A, Nawroth P, Neurath MF, Slattery T, Beach D, McClary J, Nagashima M, Morser J, Stern D, Schmidt AM (1999) RAGE mediates a novel proinflammatory axis: a central cell surface receptor for S100/calgranulin polypeptides. Cell 97:889-901

Huttunen HJ, Fages C, Rauvala H (1999) Receptor for advanced glycation end products (RAGE)-mediated neurite outgrowth and activation of NF-kappaB require the cytoplasmic domain of the receptor but different downstream signaling pathways. J Biol Chem 274:19919-19924

Huttunen HJ, Kuja-Panula J, Rauvala H (2002) Receptor for advanced glycation end products (RAGE) signaling induces CREB-dependent chromogranin expression during neuronal differentiation. J Biol Chem 277:38635-38646

Koch M, Chitayat S, Dattilo BM, Schiefner A, Diez J, Chazin WJ, Fritz G (2010) Structural basis for ligand recognition and activation of RAGE. Structure 18:1342-1352

Kusumi A, Suzuki KG, Kasai RS, Ritchie K, Fujiwara TK (2011) Hierarchical mesoscale domain organization of the plasma membrane. Trends Biochem Sci 36:604-615

Kwik J, Boyle S, Fooksman D, Margolis L, Sheetz MP, Edidin M (2003) Membrane cholesterol, lateral mobility, and the phosphatidylinositol 4,5-bisphosphate-dependent organization of cell actin. Proceedings of the National Academy of Sciences 100:13964-13969

Lander HM, Tauras JM, Ogiste JS, Hori O, Moss RA, Schmidt AM (1997) Activation of the receptor for advanced glycation end products triggers a p21(ras)-dependent mitogen-activated protein kinase pathway regulated by oxidant stress. J Biol Chem 272:17810-17814

Leclerc E, Fritz G, Vetter SW, Heizmann CW (2009) Binding of S100 proteins to RAGE: an update. Biochim Biophys Acta 1793:993-1007

Lingwood D, Simons K (2010) Lipid rafts as a membrane-organizing principle. Science 327:46-50

Lisanti MP, Scherer PE, Vidugiriene J, Tang Z, Hermanowski-Vosatka A, Tu YH, Cook RF, Sargiacomo M (1994) Characterization of caveolin-rich membrane domains isolated from an endothelial-rich source: implications for human disease. J Cell Biol 126:111-126

Logsdon CD, Fuentes MK, Huang EH, Arumugam T (2007) RAGE and RAGE ligands in cancer. Curr Mol Med 7:777-789

Matsudaira PT (1989) Strategies for obtaining partial amuni acid sequence data. In a practical guide to protein and peptide purification for microsequencing. Academic Press, New York, pp 29-30

Phair RD, Gorski SA, Misteli T (2004) Measurement of dynamic protein binding to chromatin in vivo, using photobleaching microscopy. Methods Enzymol 375:393-414

Pike LJ (2003) Lipid rafts: bringing order to chaos. J Lipid Res 44:655-667

Pucadyil TJ, Chattopadhyay A (2006) Role of cholesterol in the function and organization of G-protein coupled receptors. Prog Lipid Res 45:295-333

Reddy MA, Li SL, Sahar S, Kim YS, Xu ZG, Lanting L, Natarajan R (2006) Key role of Src kinase in S100B-induced activation of the receptor for advanced glycation end products in vascular smooth muscle cells. J Biol Chem 281:13685-13693

Ronchi P, Colombo S, Francolini M, Borgese N (2008) Transmembrane domain-dependent partitioning of membrane proteins within the endoplasmic reticulum. J Cell Biol 181:105-118

Sbai O, Devi TS, Melone MA, Feron F, Khrestchatisky M, Singh LP, Perrone L (2010) RAGE-TXNIP axis is required for S100B-promoted Schwann cell migration, fibronectin expression and cytokine secretion. J Cell Sci 123:4332-4339

Schmidt AM, Vianna M, Gerlach M, Brett J, Ryan J, Kao J, Esposito C, Hegarty H, Hurley W, Clauss M, *et al.* (1992) Isolation and characterization of two binding proteins for advanced glycosylation end products from bovine lung which are present on the endothelial cell surface. J Biol Chem 267:14987-14997

Schwab UE, Ribeiro CM, Neubauer H, Boucher RC (2003) Role of actin filament network in Burkholderia multivorans invasion in well-differentiated human airway epithelia. Infect Immun 71:6607-6609

Shaw MK, Tilney LG (1999) Induction of an acrosomal process in Toxoplasma gondii: visualization of actin filaments in a protozoan parasite. Proc Natl Acad Sci U S A 96:9095-9099

Simons K, Gerl MJ (2010) Revitalizing membrane rafts: new tools and insights. Nat Rev Mol Cell Biol 11:688-699

Spector I, Braet F, Shochet NR, Bubb MR (1999) New anti-actin drugs in the study of the organization and function of the actin cytoskeleton. Microsc Res Tech 47:18-37

Syed A, Lesoine MD, Bhattacharjee U, Petrich JW, Smith EA (2014) The number of accumulated photons and the quality of stimulated emission depletion lifetime images. Photochem Photobiol 90:767-772

Syed A, Zhu Q, Smith EA (2016) Ligand binding affinity and changes in the lateral diffusion of receptor for advanced glycation endproducts (RAGE). Biochim Biophys Acta 1858:3141-3149

Taguchi A, Blood DC, del Toro G, Canet A, Lee DC, Qu W, Tanji N, Lu Y, Lalla E, Fu C, Hofmann MA, Kislinger T, Ingram M, Lu A, Tanaka H, Hori O, Ogawa S, Stern DM, Schmidt AM (2000) Blockade of RAGE-amphoterin signalling suppresses tumour growth and metastases. Nature 405:354-360

Towbin H, Staehelin T, Gordon J (1979) Electrophoretic transfer of proteins from polyacrylamide gels to nitrocellulose sheets: procedure and some applications. Proc Natl Acad Sci U S A 76:4350-4354

van Zoelen EJ, Tertoolen LG, de Laat SW (1983) Simple computer method for evaluation of lateral diffusion coefficients from fluorescence photobleaching recovery kinetics. Biophys J 42:103-108

Veya L, Piguet J, Vogel H (2015) Single Molecule Imaging Deciphers the Relation between Mobility and Signaling of a Prototypical G Protein-coupled Receptor in Living Cells. Journal of Biological Chemistry 290:27723-27735

Wang L, Li S, Jungalwala FB (2008) Receptor for advanced glycation end products (RAGE) mediates neuronal differentiation and neurite outgrowth. J Neurosci Res 86:1254-1266

Xiong F, Leonov S, Howard AC, Xiong S, Zhang B, Mei L, McNeil P, Simon S, Xiong WC (2011) Receptor for advanced glycation end products (RAGE) prevents endothelial cell

membrane resealing and regulates F-actin remodeling in a beta-catenin-dependent manner. J Biol Chem 286:35061-35070

Yan SD, Bierhaus A, Nawroth PP, Stern DM (2009) RAGE and Alzheimer's disease: a progression factor for amyloid-beta-induced cellular perturbation? J Alzheimers Dis 16:833-843

Yan SD, Chen X, Fu J, Chen M, Zhu H, Roher A, Slattery T, Zhao L, Nagashima M, Morser J, Migheli A, Nawroth P, Stern D, Schmidt AM (1996) RAGE and amyloid-beta peptide neurotoxicity in Alzheimer's disease. Nature 382:685-691

Yeh CH, Sturgis L, Haidacher J, Zhang XN, Sherwood SJ, Bjercke RJ, Juhasz O, Crow MT, Tilton RG, Denner L (2001) Requirement for p38 and p44/p42 mitogen-activated protein kinases in RAGE-mediated nuclear factor-kappaB transcriptional activation and cytokine secretion. Diabetes 50:1495-1504

Zong H, Madden A, Ward M, Mooney MH, Elliott CT, Stitt AW (2010) Homodimerization is essential for the receptor for advanced glycation end products (RAGE)-mediated signal transduction. J Biol Chem 285:23137-23146

Figures

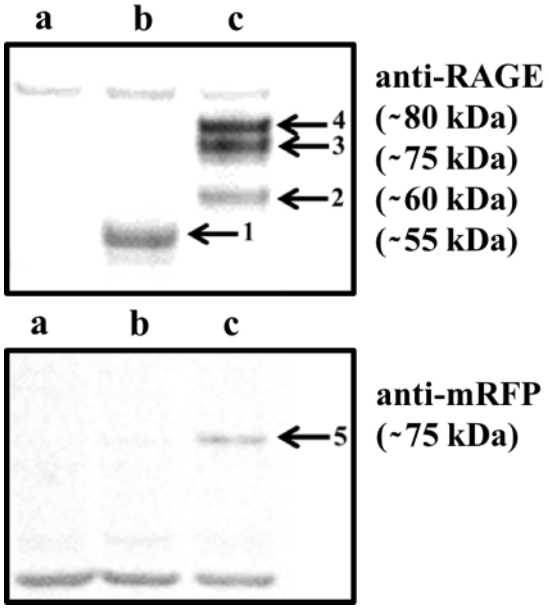

Figure 1. Western blot analysis of (a) GM07373 cell lysate, (b) GM07373-RAGE cell lysate, and (c) GM07373-RAGE-mRFP cell lysate. (Top) fluorescence image of the PVDF membrane probed with anti-RAGE antibody; (bottom) fluorescence image of the PVDF membrane probed with anti-mRFP antibody. Unlabeled bands (three upper bands in the top image and three lower bands in the bottom image) are present in all lanes and likely represent non-specific interactions of antibodies.

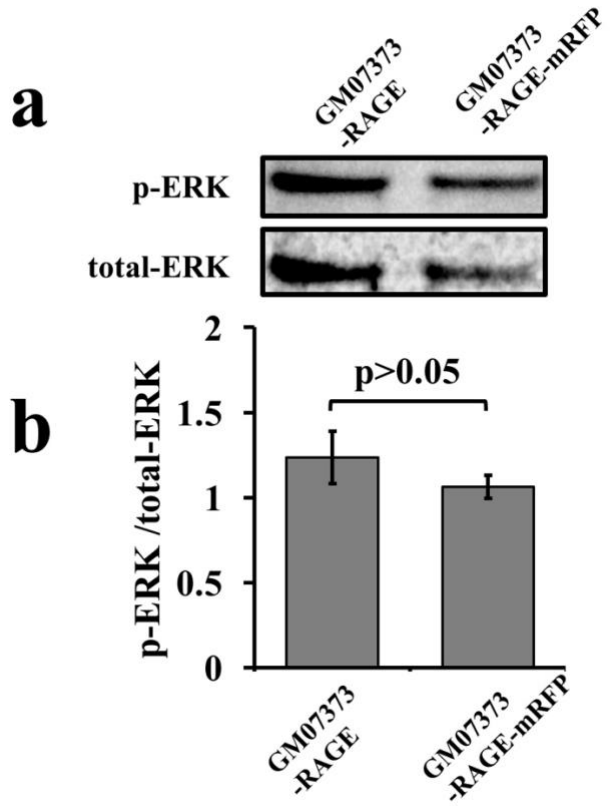

Figure 2. Western blot analysis of phosphorylation of ERK and total-ERK expression in the GM07373-RAGE cell lysate and GM07373-RAGE-mRFP cell lysate. (a) Fluorescence image of the PVDF membrane probed with anti-p-ERK or anti-total-ERK antibody. (b) Average (n = 3) fluorescence intensities of the 42 kDa band of p-ERK divided by the 42 kDa total-ERK band. Error bars represent one standard deviation.

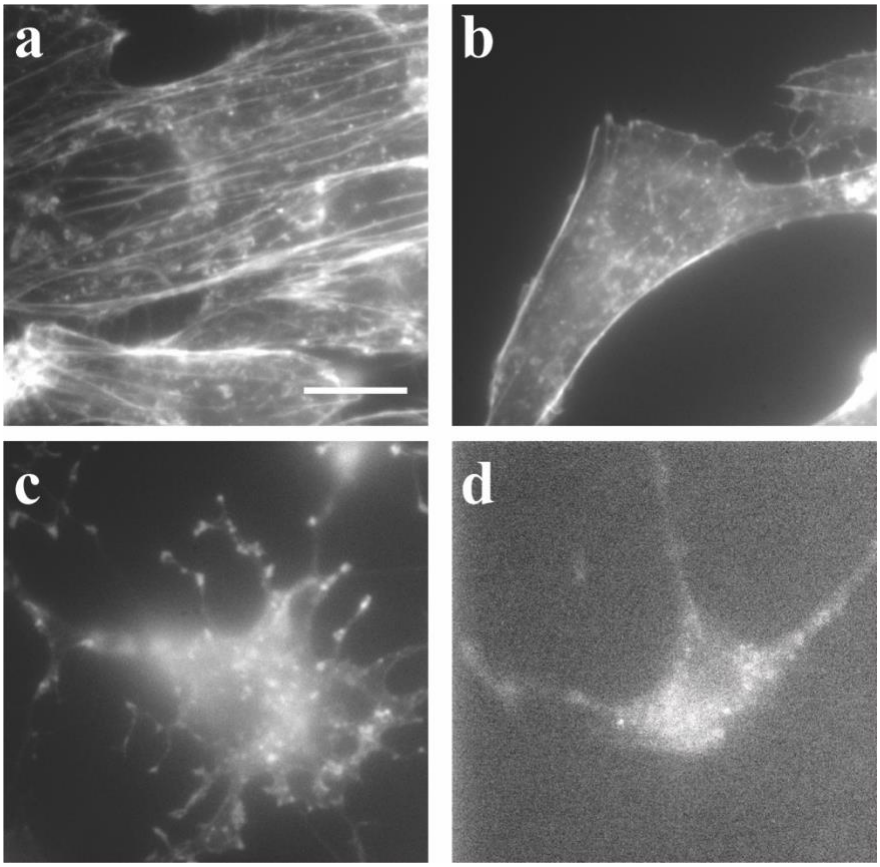

Figure 3. Fluorescence images of GM07373-RAGE cells with the actin cytoskeleton stained with Atto 647N conjugated phalloidin. (a) No treatment, (b) 5 mM methyl-β-cyclodextrin treatment, (c) 10 μM cytochalasin-D treatment, or (d) 3 μM Jasplakinolide treatment. The intensity scales are: (a) and (b) 1700 to 7000 intensity units, (c) 1500 to 3000 intensity units, and (d) 1500 to 1700 intensity units. The scale bar is 20 μm and is the same for all images.

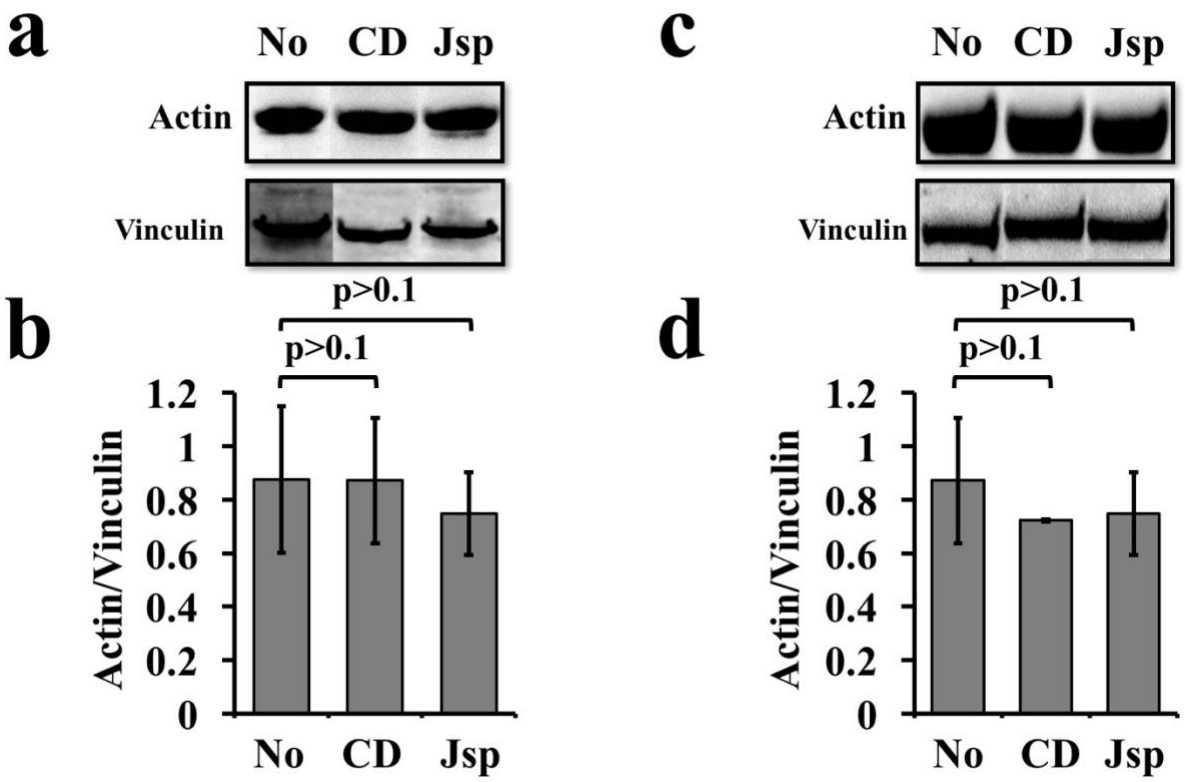

497

498 Figure 4. Western blot analysis of actin expression in the (a, b) GM07373-RAGE and (c, d)
499 GM07373 cell lysate with no treatment (No), 10 μM cytochalasin D (CD) treatment, or 3 μM
500 Jasplakinolide (Jsp) treatment. (a, c) Fluorescence image of the PVDF membrane probed with
501 anti-actin or anti-vinculin antibody. (b, d) Average (n = 3) fluorescence intensities of the actin
502 band divided by the vinculin band. Error bars represent one standard deviation.

503

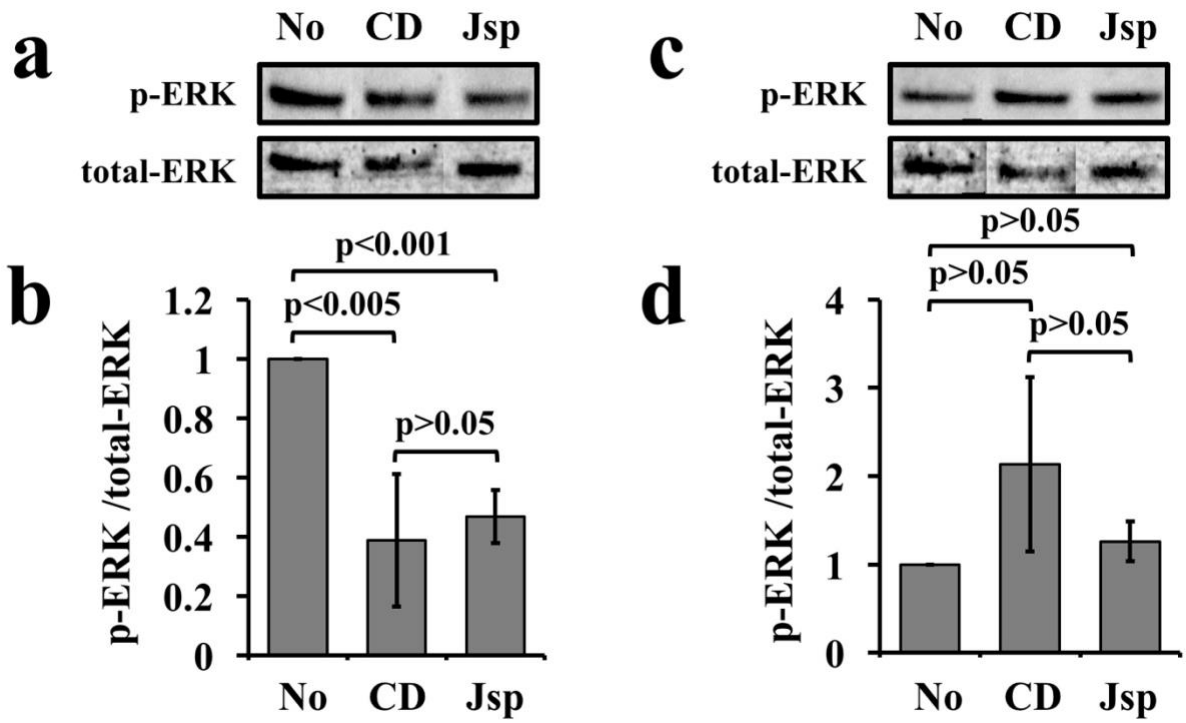

Figure 5. Western blot analysis of phosphorylation of ERK and total-ERK expression in the (a, b) GM07373-RAGE and (c, d) GM07373 cell lysate with no treatment (No), 10 μM cytochalasin D (CD) treatment, or 3 μM Jasplakinolide (Jsp) treatment. (a, c) Fluorescence image of the PVDF membrane probed with anti-p-ERK or anti-total-ERK antibody. (b, d) Average (n = 3) fluorescence intensities of the 42 kDa band of p-ERK divided by the 42 kDa total-ERK band. The band intensities were normalized to the no treatment band. Error bars represent one standard deviation.

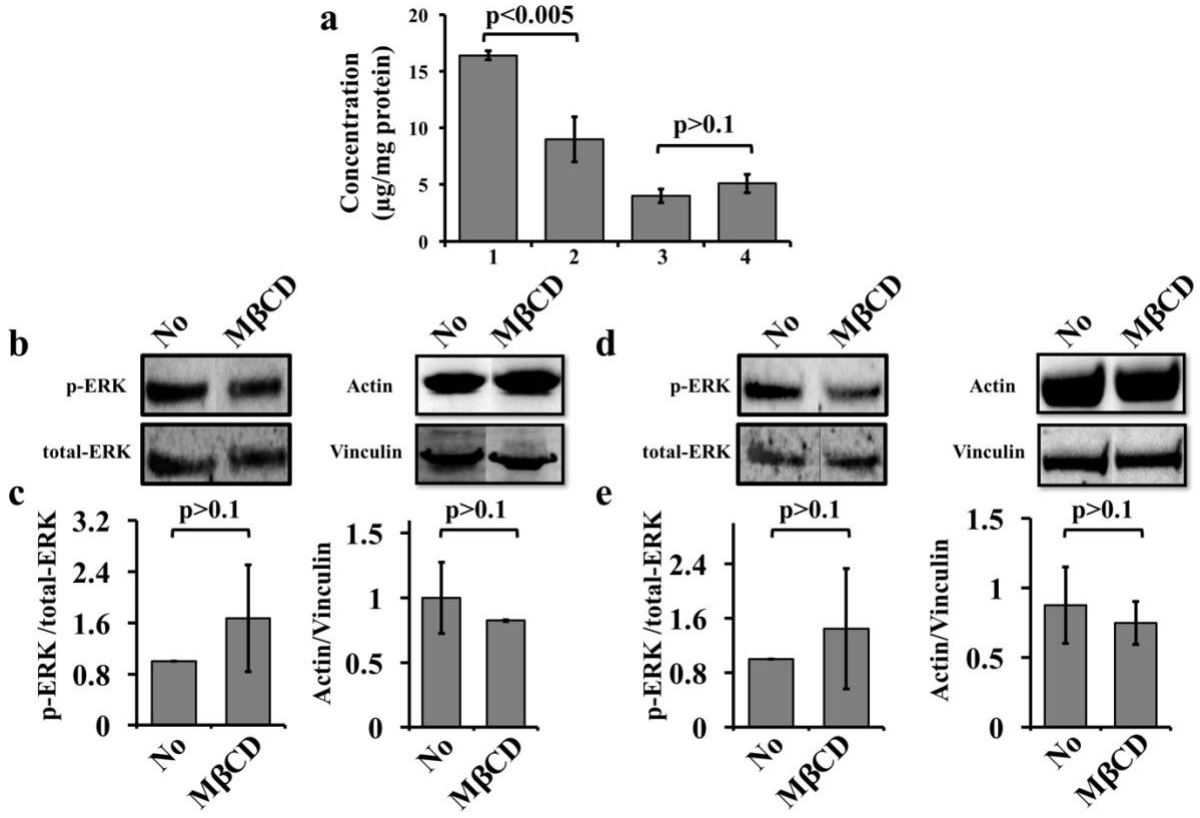

Figure 6. (a) Cholesterol quantification with Amplex® Red assay. Average (n = 2) free cholesterol (1 and 2) and cholesterol ester (3 and 4) concentration as measured from GM07373-RAGE cell lysate at native cellular conditions (1 and 3) and 5 mM methyl-β-cyclodextrin (MβCD) treated (2 and 4). Effect of MβCD treatment on (b, c) GM07373-RAGE cells and (d, e) GM07373 cells. (b, d) Fluorescence image of the PVDF membrane probed with anti-p-ERK, anti-total-ERK, anti-actin or anti-vinculin antibody. (c, e) Average (n=4) fluorescence intensities of the 42 kDa band of p-ERK divided by the 42 kDa total-ERK band (left); Average (n=2) fluorescence intensities of the actin band divided by the vinculin band (right). Error bars represent one standard deviation.

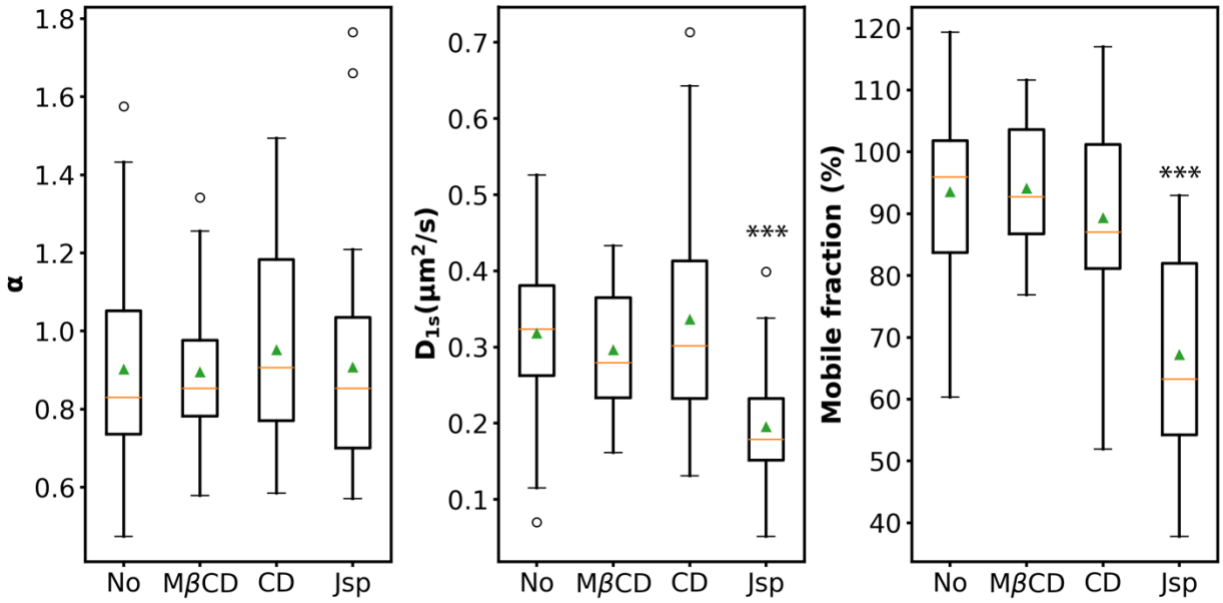

Figure 7. Box-and-whisker plots (n = 24 to 53) of RAGE-mRFP diffusion parameters in the GM07373 cell membrane obtained by FRAP after no treatment (No), 5 mM methyl-β-cyclodextrin (MβCD) treatment, 10 μM cytochalasin D (CD) treatment, or 3 μM Jasplakinolide (Jsp) treatment. The median and mean are represented as a horizontal line and triangle, respectively. The box limits are 50% (25–75%), the whiskers indicates 1.5 times the interquartile range, and the outliers are shown as open circles. *** indicates a statistically different from no treatment at the $p<0.001$ level.